UC Berkeley

Title

Mechanisms for bacterial gliding motility on soft substrates

Permalink

Journal

ISSN

Authors

Tchoufag, Joël
Ghosh, Pushpita
Pogue, Connor B
et al.

Publication Date

DOI

Peer reviewed

Mechanisms for bacterial gliding motility on soft substrates

Joël Tchoufag[a], Pushpita Ghosh[b], Connor B. Pogue[c], Beiyan Nan[c], and Kranthi K. Mandadapu[a,d,1]

[a]Department of Chemical and Biomolecular Engineering, University of California, Berkeley, CA 94720; [b]Centre for Interdisciplinary Sciences, Tata Institute of Fundamental Research, Hyderabad 500107, India; [c]Department of Biology, Texas A&M University, College Station, TX 77843; and [d]Chemical Sciences Division, Lawrence Berkeley National Laboratory, Berkeley, CA 94720

The motility mechanism of certain prokaryotes has long been a mystery, since their motion, known as gliding, involves no external appendages. The physical principles behind gliding still remain poorly understood. Using myxobacteria as an example of such organisms, we identify here the physical principles behind gliding motility and develop a theoretical model that predicts a 2-regime behavior of the gliding speed as a function of the substrate stiffness. Our theory describes the elasto-capillary–hydrodynamic interactions between the membrane of the bacteria, the slime it secretes, and the soft substrate underneath. Defining gliding as the horizontal translation under zero net force, we find the 2-regime behavior is due to 2 distinct mechanisms of motility thrust. On mildly soft substrates, the thrust arises from bacterial shape deformations creating a flow of slime that exerts a pressure along the bacterial length. This pressure in conjunction with the bacterial shape provides the necessary thrust for propulsion. On very soft substrates, however, we show that capillary effects must be considered that lead to the formation of a ridge at the slime–substrate–air interface, thereby creating a thrust in the form of a localized pressure gradient at the bacterial leading edge. To test our theory, we perform experiments with isolated cells on agar substrates of varying stiffness and find the measured gliding speeds in good agreement with the predictions from our elasto-capillary–hydrodynamic model. The mechanisms reported here serve as an important step toward an accurate theory of friction and substrate-mediated interactions between bacteria proliferating in soft media.

myxobacteria | gliding motility | mechanosensitivity | lubrication | elasto-capillary–hydrodynamics

Across the diverse range of eukaryotic and prokaryotic cells, most bacteria are found living on surfaces rather than in solutions (1–4). As a result, phenomena pertaining to both single cells (motility, morphogenesis, cell division, etc.) as well as multicellular colonies (biofilm formation and growth, durotaxis, chemotaxis, streamers formations, etc.) are fundamentally related to the presence of a surface and its interaction with cells (4, 5). For instance, in the case of myxobacteria, a complex coupling between their intrinsic motility and their underlying substrate regulates their ability to form biofilms in the presence of nutrients or to aggregate into fruiting bodies in starvation conditions (6). Inspection of a swarm of myxobacteria, such as *Myxococcus xanthus*, reveals 2 types of motility: social (S)-motility or "twitching" involving type IV pili, and adventurous (A)-motility or "gliding" occurring without any external appendage (7). In order to explain the above-mentioned complex phenomena ranging from single-cell motility to emergent collective behaviors responsible for biofilm formation, bacteria–surface interactions (hydrodynamics, adhesion, biochemistry, etc.) must be understood.

In the present work, we seek to shed light on the physical principles behind gliding motility and the nature of the interaction between a gliding A-motile cell and its substrate. Indeed, it has been long reported that the spreading rate of a myxobacteria colony depends on the substrate stiffness (8, 9): an effect known as mechanosensitivity. However, while there exist some physical models for the mechanosensitivity of eukaryotic cells in tissues due to adhesion (10), the mechanism of myxobacterial gliding and its dependency on the substrate stiffness remains unclear mainly due to the existence of a thin slime layer secreted between the cell and the substrate (11). The physical approaches that have been previously undertaken to explain myxobacteria gliding are either on the molecular scale or continuum models on the scale of the whole cell (12). The former is primarily concerned with identifying genes, proteins, and molecular motors and their role in empowering a cell to glide (7, 13–15). Here, our focus is not to elucidate the internal molecular mechanisms (15–19) but rather to identify the physical principles governing the gliding motion of myxobacteria and how they interact with their environment. As such, our theory belongs to the class of models analyzing the bacteria at the cellular level.

To the best of our knowledge, the physical forces behind gliding of prokaryotes at the cellular level can be classified under 4 categories: osmotic forces, surface-tension gradients, slime secretion, and traveling waves. There are excellent reviews that describe each of these mechanisms for different gliding organisms (7, 20, 21). It suffices here to say that in the case of myxobacteria, 2 models are repeatedly invoked in attempting to explain the physical mechanism behind gliding at the cellular level. The first model, known as the slime-extrusion model, suggests that myxobacteria glide by secreting their slime via

---

Significance

Gliding motility is the ability of certain rod-shaped bacteria to translocate on surfaces without the aid of external appendages such as flagella, cilia, or pili. This motility is crucial to their developmental cycle because it regulates their proliferation in the presence of nutrients or aggregation to form fruiting bodies in starvation conditions. Using myxobacteria as a canonical example of these organisms, we show that single-cell gliding is mediated by elastic, viscous, and capillary interactions between the bacteria, the slime it secretes, and the substrate underneath. Our theory reproduces well-measured speeds of *Myxococcus xanthus* cells on surfaces of varying stiffness and provides an explanation for the sensitivity of cell spreading to the substrate mechanics, a common feature across bacteria.

---

extrusion nozzles at the lagging pole, similar to a jet that propels through fuel ejection (12, 22). However, recent experiments have shown that the thrust-generating complex motors are distributed all along the cell rather than being concentrated at the lagging pole (23, 24). Moreover, slime was still found to be secreted underneath the surface of *M. xanthus* mutant cells, which are nonmotile, thereby showing that the production of slime does not necessarily lead to bacterial gliding (11). For these reasons and others (for a review, see ref. 7), the slime-extrusion model has now been disproved and is obsolete.

The second model, built at the scale of the entire cell, is based on waves propagating on the bacterial surface and the slime acting as a thin lubricating fluid. First developed for another gliding organism, namely Flexibacter (25), this model has been applied to myxobacteria with various complex rheological behaviors for the slime (26–28). However, these studies all consider the substrate to be a rigid wall and are thus in essence unable to explain the mechanosensitivity feature of myxobacteria reported by many experiments (8, 9, 29). Moreover, all of the aforementioned studies as well as recent agent-based models (24, 30) prescribe the bacterial speed and, therefore, do not explain the physical mechanisms leading to gliding and self-propulsion. In this work, we focus on uncovering the physical mechanisms behind the gliding motion of myxobacteria without any appendages on soft and deformable substrates. In doing so, we identify 1) the physical nature of the forces between the bacteria and the surface, namely elastic, capillary, and hydrodynamic interactions; 2) the interplay between these forces leading to a nonzero gliding speed; and 3) how the speed depends on the substrate softness (mechanosensitivity).

An Elasto-Hydrodynamic Mechanism Governs Bacterial Gliding on Mildly Soft Substrates

Our model is built upon 2 essential features established through previous experiments on myxobacteria. The first feature is the geometry of the cell's basal surface that interacts with the substrate. As recently revealed through total internal reflection fluorescence (TIRF) microscopy experiments of *M. xanthus* cells (24), this basal surface possesses an oscillatory structure that we approximate by a sinusoidal shape $b(x,t)$ (Fig. 1). The TIRF experiments were carried out on cells expressing green fluorescence protein (GFP) in the cytoplasm and yet showed a modulation of intensity with a period of $L \sim 1\mu$m (24) (similar to the periodicity of localization of MreB filaments; see refs. 19 and 31). Given that GFP was evenly distributed in the cytoplasm, the TIRF images are thus evidence that the distance from the cytoplasm to the microscope glass is modulated. Images from atomic force measurement also revealed that surfaces of single *M. xanthus* cells display a helical pattern (32). Such shape deformation, which arises from the assembly and aggregation of the motility complexes at the so-called "focal-adhesion sites," may therefore be a necessary condition for gliding (15, 24, 33). The second feature is that myxobacteria gliding is always accompanied by a trail of slime in the wake of the motile cells (11, 34). Using microscopy with wet surface-enhanced ellipsometry contrast, a thin layer of slime was observed underneath the basal cell surface of even nonmotile mutants (11). Slime deposition was thus suggested to be a general means for gliding organisms to adhere to and move over surfaces. Recently, the stick–slip dynamics of twitching *M. xanthus* cells was also well explained by understanding the slime to function both as a glue and as a lubricant (35). Here, we corroborate these findings and demonstrate that the slime acts as a crucial agent that not only lubricates the motion of myxobacteria but also creates a coupling between the cell and the deformable substrate.

The Slime Film Lubricates the Bacterial Gliding Motion. To model the slime-mediated interaction between myxobacteria and their
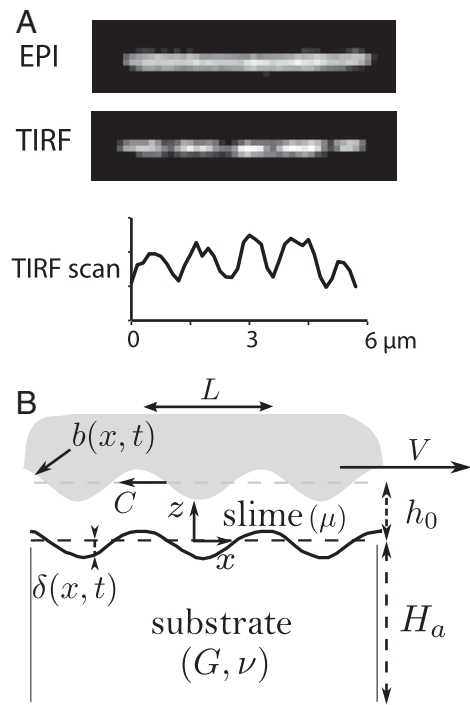

Fig. 1. (*A*) Epifluorescence and TIRF microscopic images of the surface of a single *M. xanthus* cell. The TIRF scan shows how the bacterial surface has a quasiperiodic structure with a wavelength ∼1.2 μm. (*B*) Schematic description: a side view of a gliding bacterium (in gray) with a sinusoidal basal shape that represents the bacterial surface undulations revealed by TIRF microscopy. The contact with the soft substrate is lubricated by a thin film of slime. See the text for a description of the variables.

substrate, we make the following assumptions. We consider small shear rates of the exopolysaccharide (EPS) slime and hence treat it as a newtonian viscous fluid, despite its polymeric constitution (11). The good comparison of our model with experiments will justify a posteriori that the nonnewtonian rheology of the slime has a second-order influence on the myxobacteria–substrate interaction. Furthermore, we neglect inertial effects given that for the characteristic speed $V \sim 2\,\mu$m/min (35), mean height of the interstitial gap between the bacteria and the substrate $h_0 \sim 10$ nm (11), and large viscosity of bacterial EPS $\mu \sim 5$ to 20 Pa.s (36, 37), the typical Reynolds number is $Re \ll 1$ as in the locomotion of most microorganisms (38). Hence, we model the dynamics of the slime using the Stokes equations (39). Given the geometric ratio of the interstitial gap $\epsilon := \dfrac{h_0}{L} \sim 10^{-2} \ll 1$, we use the classical lubrication approximation (40, 41) for the slime film and further simplify the Stokes equations. Moreover, ignoring the rotation of the myxobacteria along its long axis, we confine the problem to 2 dimensions. Lastly, we account for the deformation $\delta(x,t)$ of the soft substrate, caused by the pressure in the lubricating slime (Fig. 1*B*). The total thickness of the slime layer is thus $[h(x,t) - \delta(x,t)]$, where $h(x,t) = h_0 + b(x,t)$. With these simplifications, the Stokes equations can be reduced to a modified form of the so-called Reynolds equation (40, 41), governing the dynamics of the lubricating film of slime and given by (*Materials and Methods* and *SI Appendix, section 1.2*)

$$-\frac{\partial}{\partial t}(h-\delta) + \frac{\partial}{\partial x}\left[\frac{1}{12\mu}\frac{\partial p}{\partial x}(h-\delta)^3 + \frac{1}{2}V(h-\delta)\right] = 0, \quad \textbf{[1]}$$

where $p(x,t)$ is the pressure in the slime and V is the gliding velocity of the bacteria that remains to be solved for.

The Slime Equation Admits Traveling Wave Solutions Compatible with Bacterial Shape Deformations. In the frame of reference translating with the cell, we consider the propagation of a traveling wave along the cell surface (24) as several recent experiments report gliding is strongly correlated with molecular motor complexes moving with helical trajectories on a scaffold provided by MreB actin (15, 17, 19, 24, 42). Some of these motor complexes were observed to slow down once they arrive at the basal cell boundary, in contact with the substrate. Due to their low velocity, when observed using regular microscopy, they appear almost stationary (15, 17, 23, 24), corresponding to a traveling disturbance on the cell surface in the reference frame translating with the bacteria. When viewed externally, the motors appear to drive the rotation of a helical structure that generates transverse waves on the ventral surface (15, 17, 24). Certainly, the slime-lubrication equation, given by Eq. **1**, admits such traveling wave solutions as we now establish.

Let us consider a membrane carrying a unidirectional traveling wave of speed C, such that the shape $h(x,t)$ satisfies

$$\frac{\partial h}{\partial t} = C\frac{\partial h}{\partial x}. \qquad [2]$$

Assuming the x axis is oriented positively to the right as in Fig. 1*B*, positive and negative values of C correspond to left and right traveling waves, respectively. To obtain traveling wave solutions of Eq. **1**, we search for a substrate-deformation field that also satisfies $\frac{\partial \delta}{\partial t} = C\frac{\partial \delta}{\partial x}$, where we assume that the substrate deformation exhibits traveling waves of the same speed as that of the bacterial surface. Using this ansatz, Eq. **1** can be rewritten as (*SI Appendix*, section 1.3)

$$\frac{\partial}{\partial x}\left[\frac{\partial p}{\partial x}(h-\delta)^3 + 6\mu(V-2C)(h-\delta)\right] = 0. \qquad [3]$$

According to Eq. **3**, the pressure distribution in the slime layer depends (nonlinearly) on the substrate deformation $\delta(x,t)$, which we now set out to determine.

The Substrate Surface Deforms Elastically during Bacterial Gliding Motion. In many situations, the horizontal and vertical length scales of the substrate are on the order of centimeters and millimeters, respectively (43). Since both dimensions are much larger than the typical length of myxobacteria, we can represent the substrate as a semiinfinite medium. Moreover, gel substrates are generally viscoelastic, where the relative importance of viscous to elastic effects depend on the frequency of excitation of the material. Here, the characteristic frequency is that of the traveling disturbance $f = C/L \approx 0.32\mu\mathrm{m.s}^{-1}/1\mu\mathrm{m} = 0.32$ Hz, where the estimated wave speed corresponds to the experimental speed of the slow AlgR molecules (17), which are essential components in the motor complexes. In the case of agar gels at moderate to high concentrations ($\geq 1\%$) and at such frequencies, the loss modulus is expected to remain smaller than the storage modulus by one or more orders of magnitude (44). Therefore, we first treat the substrate as a purely elastic half-space. Furthermore, we formulate the problem in the context of linear elasticity (small deformations) and make the quasistatic assumption that the time-dependent solution can be found by solving a static problem at every instant. In this framework, the deformation of the substrate surface under the action of the film pressure is given by (*SI Appendix*, sections 2.1–2.5)

$$\delta(x,t) = \frac{(1-\nu)}{\pi G}\int_{-\ell/2}^{\ell/2} p(x',t)\ln\frac{|x-x'|}{x_0}\mathrm{d}x'. \qquad [4]$$

Here, ℓ is the length of the entire bacteria. In Eq. **4**, x_0 is a constant that sets the zero displacement point on the substrate (45), and $G = E/2(1+\nu)$ is the shear modulus for Young modulus E and Poisson ratio ν. Note that we restrict our analysis to incompressible substrates, for which $\nu = 1/2$, in order to ensure that the deformation of the substrate surface occurs in the vertical direction only (*SI Appendix*, section 2.5). A motion in the horizontal direction would imply a slip velocity at the slime–substrate interface, in contradiction with the no-slip condition assumed earlier in the slime lubrication model Eq. **1**.

The Elasto-Hydrodynamic Model Can Be Parametrized by a Single Nondimensional Variable: The Softness Number. In order to compare the viscous and elastic forces at play in the problem, we rewrite the equations in their dimensionless forms. To that end, we first note that the characteristic deformation scale of the substrate reads $\Delta = (1-\nu)PL/G$, where $P = \mu CL/h_0^2$ is the characteristic pressure scale (*SI Appendix*, section 3). This can then be used to nondimensionalize the thickness of the slime layer to yield $(h-\delta) = h_0\left(\hat{h} - \eta\hat{\delta}\right)$, where $\hat{h} = h/h_0$, $\hat{\delta} = \delta/\Delta$. Here, $\eta = \Delta/h_0$ is a dimensionless number that compares the characteristic deformation of the substrate due to the slime pressure to the mean thickness of the film.

For a given cell shape, η essentially captures the influence of the substrate deformability on variations of the lubrication gap during gliding. Therefore, it is also known as the softness parameter and be recast as (46, 47)

$$\eta = \frac{(1-\nu)PL}{Gh_0}, \qquad [5]$$

such that increasingly larger values of η denote increasingly softer substrates. Using the above dimensionless parameters and defining $\hat{p} = p/P$, $\hat{x} = x/L$, $\hat{t} = t/(L/C)$, $\hat{V} = V/C$, and $n = \ell/L$, the governing equations for the slime film and the substrate deformation can be recast in a dimensionless form (*Materials and Methods* and *SI Appendix*, section 3).

Bacterial Gliding Motion Occurs under Zero Lift and Drag Forces. In order to obtain the slime pressure at different values of the softness parameter η, we specify 2 boundary conditions such that Eq. **3** admits a unique solution. We first set $\hat{p}(n/2,\hat{t}) = 0$. In other words, we assume that the slime pressure at the leading edge of the cell drops to the atmospheric (zero) pressure. Second, given that myxobacteria move without inertia in the Stokes regime and that the forces for gliding result from the internal motors, the sum of the external forces on the cell must vanish according to Newton's second law. In the $\hat{z}$ direction, this implies that the lift force from the film pressure must vanish. In the lubrication approximation, this lift-free condition reads (*SI Appendix*, section 4)

$$\int_{-n/2}^{n/2} \hat{p}(\hat{x},\hat{t})\mathrm{d}\hat{x} = 0, \qquad [6]$$

and, consequently, the second boundary condition for Eq. **3** is a global condition. In the $\hat{x}$ direction, the drag-free condition provides an equation, which must be inverted to obtain the gliding speed V (*SI Appendix*, section 4)

$$-\int_{-n/2}^{n/2}\left(\hat{p}\frac{\partial \hat{b}}{\partial \hat{x}} + \frac{1}{2}\frac{\partial \hat{p}}{\partial \hat{x}}\left(\hat{h} - \eta\hat{\delta}\right) + \frac{\hat{V}}{\hat{h} - \eta\hat{\delta}}\right)\mathrm{d}\hat{x} = 0. \qquad [7]$$

The lift-free and drag-free constraints, i.e., Eqs. **6** and **7**, together define the gliding motion of myxobacteria at the cellular level.

Note that having imposed the shape of the bacteria, we can ignore the zero-torque condition, as commonly seen in the studies of swimming sheets (48–50). An alternative would consist in solving for the bacterial membrane shape under the requirement that its bending and tensile stresses balance those due to the slime and those imposed by the internal motors (51). However, in such an approach, one must postulate the form of the torque applied by the traveling motors.

The system of coupled Eqs. **3**, **6**, and **7**, along with the condition $\hat{p}(n/2, \hat{t}) = 0$, admits a unique solution $\mathbf{q}(\hat{x}, \hat{t}) := [\hat{p}(\hat{x}, \hat{t}), \hat{\delta}(\hat{x}, \hat{t}), \hat{V}(\hat{t})]^T$ for a given softness number η and a given geometry of the basal cell shape. In the case of myxobacteria, images of myxobacteria obtained with TIRF microscopy (Fig. 1A) indicate that the basal cell geometry can be approximated, in 2 dimensions, by a sinusoidal shape. Therefore, throughout this study, we consider sinusoidal basal shapes of the form $b(x, t) = A \sin\left[\frac{2\pi}{L}(x + Ct)\right]$, corresponding to the dimensionless height $\hat{h}(\hat{x}, \hat{t}) = 1 + \hat{A} \sin\left[2\pi(\hat{x} + \hat{t})\right]$, where the amplitude is nondimensionalized by h_0. As such, it must satisfy $\hat{A} \in [0, 1]$ for a thin film to exist between the cell and the substrate.

We solve the problem numerically for a given η and $\hat{h}(\hat{x}, \hat{t})$ and obtain $\mathbf{q}(\hat{x}, \hat{t})$ at different instants. Due to the time periodicity of the bacterial membrane, we expect $\mathbf{q}(\hat{x}, \hat{t})$ to be periodic, hence the gliding speed as well (*SI Appendix*, section 5.4). A net gliding motion only then exists when the mean velocity, averaged over a wave period, is nonzero. Therefore, the results hereafter will be presented in their time-averaged form, expressed by the notation $\langle \cdot \rangle$.

First Result: Elasto-Hydrodynamics Dictates That the Gliding Speed Decreases to Zero as Substrates Become Softer. Fig. 2 shows the average gliding velocity as a function of the softness parameter for different amplitudes of the basal cell shape. Clearly, the gliding velocity decreases with the softness parameter η. For very small values of η, the substrate is a very stiff solid and we recover the prediction of the speed of a periodic wavy sheet (Taylor's swimmer; see ref. 48) near a rigid wall. As one could expect, the precision of this agreement improves with n, since the bacterial length increases (L being fixed) and hence its approximation by a periodic wavy sheet (*SI Appendix*, section 5.5). Indeed, it is known that in the lubrication regime near a rigid wall ($1/\eta \to \infty$), small amplitude wavy membranes have a swimming velocity given by (50, 52):

$$\left\langle \hat{V}_{\eta=0} \right\rangle = \frac{3}{2 + 1/\hat{A}^2}, \qquad \textbf{[8]}$$

which corresponds to the asymptotic values of the small-η plateaus in Fig. 2. Since $\hat{A} = A/h_0$, increasing the dimensionless amplitude is equivalent to decreasing the mean gap h_0. Therefore, we recover the well-known result that the locomotion speed of a wavy sheet increases as it approaches a rigid boundary (52). In our context, this conclusion is equivalent to stating that on stiff but elastically deformable substrates, the gliding motility speed increases with the deformation amplitude of myxobacterial membrane. However, as we increase the softness parameter, the gliding velocity transitions from a nonzero value for very stiff substrates to zero in the limit of very soft substrates. For all amplitudes $\hat{A}$, Fig. 2 shows that substantial deviations from the rigid wall solution occur when the substrate number $\eta \approx 1$, which corresponds to a substrate whose deformation is comparable to that of the slime thickness.

Second Result: Bacterial Gliding on Mildly Soft Substrates Requires That Energy Be Converted from Shape Deformations to Viscous Slime Flow. The vanishing nature of the gliding speed in the limit $\eta \to \infty$ can be understood by analyzing the horizontal force
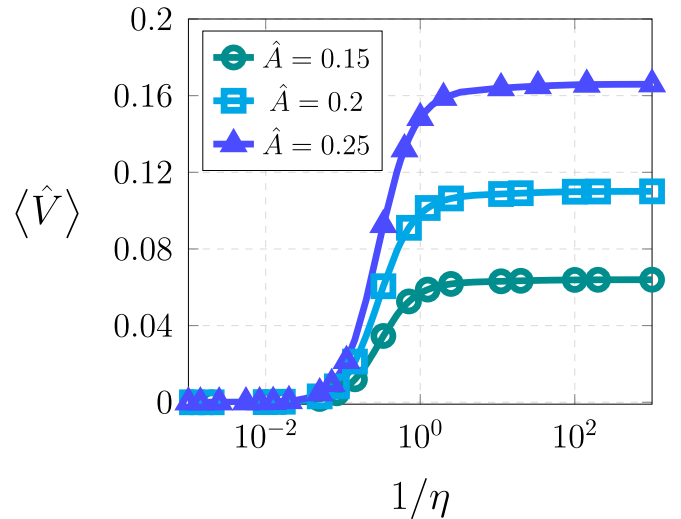

Fig. 2. Time-averaged gliding speed as function of the softness parameter for different amplitudes of the bacterial shape. Here, we consider a bacterial shape with 5 wavelengths, i.e., $n = 5$. The gliding speed increases with the substrate stiffness and with the amplitude of the bacterial shape.

balance that must be satisfied for gliding to occur. Defined by Eq. **7**, this force balance involves 3 contributions, $I_1(\hat{x}, \hat{t})$, $I_2(\hat{x}, \hat{t})$, and $I_3(\hat{x}, \hat{t})$, given by

$$I_1 = -\hat{p} \frac{\partial \hat{b}}{\partial \hat{x}}, \quad I_2 = -\frac{1}{2} \frac{\partial \hat{p}}{\partial \hat{x}} \left(\hat{h} - \eta \hat{\delta} \right), \quad I_3 = \frac{-\hat{V}}{\hat{h} - \eta \hat{\delta}}. \qquad \textbf{[9]}$$

Firstly, I_1 represents the action of the slime pressure on the bacteria induced by variations of the bacterial geometry. Hence, it vanishes for bacteria with spatially uniform shapes. Secondly, I_2 denotes the effect of pressure variations along the bacteria and would vanish in the absence of pressure gradients. Lastly, I_3 constitutes the resistance experienced by the bacteria as it must shear the slime to achieve gliding.

We show in Fig. 3 the time-averaged spatial distribution of the components I_1, I_2, and I_3 along the length of the bacteria, for 3 values of the softness parameter $\eta \in \{0.001, 5, 1000\}$. For the input parameters corresponding to Fig. 3 A, B, and C, we provide Movies S1, S2, and S3, respectively (also see *SI Appendix*, section 5.7), illustrating the dynamics of the bacterial membrane, the slime pressure field, and the deformation of the substrate surface. Fig. 3 shows, as expected, that $\langle I_3 \rangle$ is always negative and contributes to the friction experienced by the bacteria. Next, regarding the component $\langle I_2 \rangle$, its integral over the bacterial basal shape is negative and thus constitutes an additional contribution to friction. Lastly, Fig. 3 shows the term $\langle I_1 \rangle$ is positive over the length of the bacteria and provides the necessary thrust balancing the Poiseuille and Couette frictions from $\langle I_2 \rangle$ and $\langle I_3 \rangle$, respectively. Fig. 3 therefore reveals the decrease of the gliding speed with the softness number η is correlated to that of the local thrust generation along the bacteria. This can be explained in the following manner. For small values of η, the substrate is very stiff and remains almost unperturbed by the oscillations of the bacterial surface (Movie S1 and *SI Appendix*, section 5.7). This implies the thickness of the gap between the bacterial surface and the substrate oscillates and induces a lubricating flow of slime exerting on the cell-pressure oscillations in phase with the bacterial shape (*SI Appendix*, section 5.6). The resulting flow of slime exerts the thrust $\langle I_1(\hat{x}) \rangle$ along the bacteria, which leads to a nonzero gliding speed $\langle \hat{V} \rangle$. Therefore, this mechanism of thrust generation, whereby the shape oscillations are converted into a lubrication flow of slime,
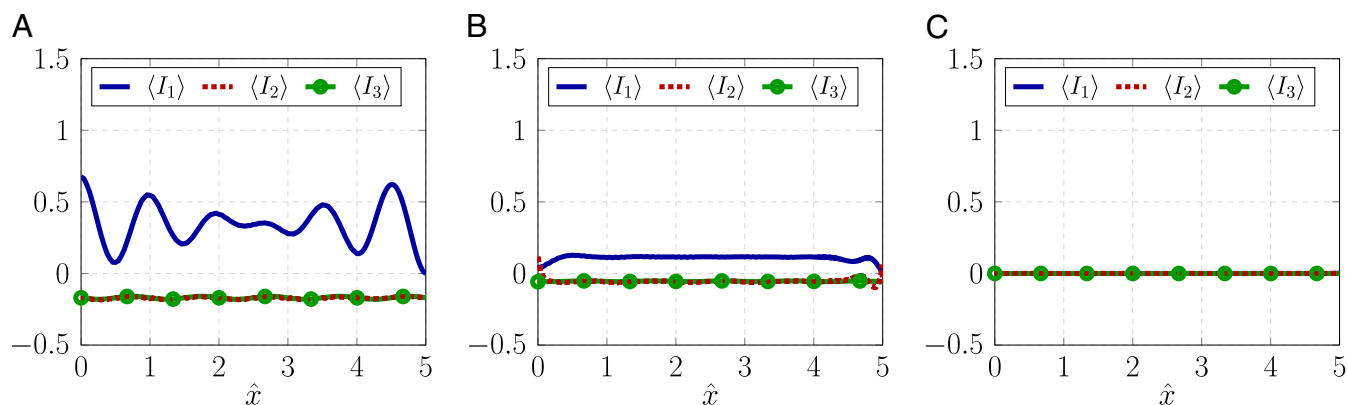
Fig. 3. Time-averaged distribution of the contributions I_1, I_2, and I_3 to the horizontal force balance for different values of η. The softness parameters are $\eta = 0.001$ (very stiff substrate) (*A*), $\eta = 5$ (mildly soft substrate) (*B*), and $\eta = 1000$ (very soft substrate) (*C*). Here, the input parameters are $\hat{A} = 0.25$ and $n = 5$.

requires little to no deformation of the substrate. As such, it cannot be sustained for very soft substrates, when $\eta \to \infty$. In fact, in this limit, the substrate is very compliant and instantaneously conforms to the oscillating bacterial surface so that $\eta\hat{\delta} \approx \hat{b}$, as supported by our computations (*SI Appendix*, sections 5.6 and 5.7 and Movie S3). Given that $\hat{p} \sim \hat{\delta} \approx \hat{b}/\eta$, the pressure distribution along the bacteria thus decays to zero as $\eta \to \infty$, thereby leading to a vanishing pressure gradient as well. Therefore, the pressure-dependent terms $\langle I_1(\hat{x})\rangle$ and $\langle I_2(\hat{x})\rangle$ tend to zero (as $\sim 1/\eta$) in the limit of very soft substrates. As a result, the gliding speed $\langle \hat{V}\rangle$ of the force-free bacteria tends to zero in the limit $\eta \to \infty$.

However, this large-η behavior is not corroborated by our experiments, which instead show the gliding speed to be quasiconstant as the softness increases, so that *M. xanthus* cells glide even on extremely soft substrates (see Fig. 8). Such a remarkable feature shows that modeling the substrate as a pure elastic half-space breaks down for large values of the softness parameter.

Motility on Very Soft Substrates Must Account for Capillary Effects

For very soft substrates, surface-tension effects can no longer be ignored in creating the substrate deformation $\hat{\delta}(\hat{x}, \hat{t})$. The elasto-capillary balance of the substrate is particularly critical at the leading edge of the bacteria. In fact, the slime–air interfacial tension can generate, from the soft substrate, a "ridge" (Fig. 4), which takes a shape determined by the balance of tensions at the substrate–slime–air triple line (*SI Appendix*, section 6.3).

Elasto-Capillary–Hydrodynamic Model. Capillary ridges are well-documented in the literature of soft solids (53–57). Here, we consider that the growth of such a ridge creates a curvature of the slime–air interface, inducing a pressure difference at the leading edge of the cell. If the capillary effects are important, then the zero-pressure condition at the leading edge, $\hat{p}(n/2, \hat{t}) = 0$, no longer holds. This pressure must be obtained within an elasto-capillary–hydrodynamic framework, as we now set out to describe. Following the work by Limat (58) and Dervaux and Limat (59), we show that the substrate deformation, formerly given by Eq. **4**, now takes the form (*SI Appendix*, sections 6.1 and 6.2)

$$\delta(x,t) \approx \frac{(1-\nu)}{\pi G} \int_{-\ell/2}^{\ell/2} p(x',t) \ln \frac{|x-x'|+\ell_s/\pi}{x_1} \mathrm{d}x'. \quad \textbf{[10]}$$

In Eq. **10**, x_1 is a constant that sets the zero displacement point on the substrate (45), and ℓ_s is a length scale below which capillary stresses at the slime–substrate interface dominate over the elastic stresses in the bulk of the substrate. Rewriting ℓ_s in dimensionless form, we obtain the elasto-capillarity number defined as

$$\xi = \frac{\ell_s}{L} = \frac{2\gamma_s(1-\nu)}{GL}, \quad \textbf{[11]}$$

where γ_s is the slime–substrate surface tension. Therefore, small (resp. large) values of ξ correspond to substrates whose surface deformations are governed by elastic (resp. capillary) stresses.

Furthermore, we can write the force balance at the capillary ridge (59) and use Laplace's law across the slime–air interface to find the leading-edge pressure (*SI Appendix*, sections 6.3 and 6.4). In the limit of small deformations, we obtain the pressure at the leading edge in the form $\hat{p}(n/2) = \mathcal{P}(\epsilon, \mathcal{R}, \hat{a}, \xi, Ca)$. In this relation, ϵ is the lubrication parameter, $\mathcal{R} = \gamma/\gamma_s$ is the ratio of the slime–air and slime–substrate interfacial tensions, and $\hat{a}$ is a measure of the slime–air interfacial thickness (56, 61). Lastly, Ca is a capillary number comparing viscous to interfacial forces at the tip of the bacteria and defined by

$$Ca = \frac{\mu C}{\gamma}. \quad \textbf{[12]}$$

The function $\mathcal{P}$, defining the leading-edge pressure, accounts for both elastic and capillary effects for all values of the substrate softness. For very stiff substrates, the elasto-capillarity number
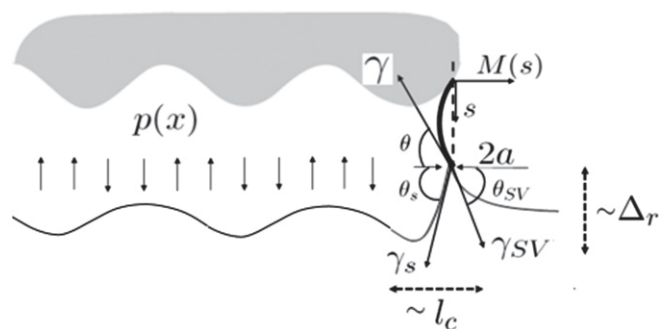

Fig. 4. Schematic description of the elasto-capillary–hydrodynamic problem: a gliding bacterium (in gray) with a sinusoidal ventral shape. A ridge is formed and balanced by the surface tensions at the slime–air, substrate–slime, and air–substrate interfaces. See the text for a description of the variables.

$\xi \to 0$ and we recover $\hat{p}(n/2, \hat{t}) \approx 0$, as previously assumed in the elasto-hydrodynamic model void of capillary effects. Likewise, the substrate deformation converges to that of a purely elastic half-space (*Materials and Methods* and *SI Appendix, section 6.5*).

For extremely soft substrates, the substrate deformation is dominated by the slime–substrate interfacial tension so that the elasto-capillary length is much larger than the bacterial length, i.e., $\xi L \gg nL$. Using this information, we find in particular that the tip pressure is negative and inversely proportional to the capillary number (*SI Appendix, section 6.5*). In other words, when Ca is small, there exists at the leading edge a strong localized-pressure sink, as hypothesized. This pressure pulls a ridge with a characteristic height (Δ_r) and extent (l_c) as indicated in Fig. 4. The length scale l_c hence represents a threshold below which the localized capillary pressure is significant. Assuming $l_c \ll L$, the force-free condition in the gliding direction reduces to the balance between I_2 and I_3, that is, between the Poiseuille-like and Couette-like forces. This conclusion is supported by the simulations of the full elasto-capillary–hydrodynamic equations as shown in Fig. 5, which shows the contributions of I_1, I_2, and I_3 to the horizontal force balance. For the input parameters corresponding to Fig. 5 *A, B,* and *C,* we provide Movies S4, S5, and S6, respectively (also see *SI Appendix, section 8.7*), illustrating the dynamics of the bacterial membrane, the slime pressure field, and the substrate surface deformation during motion.

Third Result. Bacterial gliding on very soft substrates is mediated by a localized strong pressure gradient near the leading edge of the cell

The comparison between Figs. 3*A* and 5*A* shows that for very stiff substrates, the full solution reduces to that obtained by considering only the elasto-hydrodynamic interactions. This conclusion is also supported by comparing the instantaneous dynamics of bacterial gliding on stiff substrates with and without consideration of capillary effects (Movies S1 and S4 and *SI Appendix, sections 5.7 and 8.7*). However, as the softness increases, Fig. 5 *B* and *C* shows the growing effect of the leading-edge pressure. While I_3 still contributes to a Couette-like friction, the term I_2 is now responsible for a nonzero thrust, largely due to the localized strong pressure gradient at the tip of the myxobacteria (Movie S6 and *SI Appendix, section 8.7*). In the capillarity-dominated regime ($n \ll \xi \to \infty$), we derive an asymptotic expression for the gliding speed on very soft substrates $\hat{V}_{\eta=\infty}$, as (*SI Appendix, section 6.5*)

$$\hat{V}_{\eta=\infty}(\hat{t}) \approx 2 - \Delta\hat{p}\frac{(1-\alpha)}{\beta} + \alpha, \qquad [13]$$

where $\Delta\hat{p}$ is the pressure difference between the leading and trailing edges of the cell, while α and β are factors related to the total slime layer thickness ($\hat{h} - \eta\hat{\delta}$). Since the leading-edge pressure is inversely proportional to the capillary number, so is the asymptotic velocity $\hat{V}_{\eta=\infty}$, according to Eq. **13**. In fact, a more detailed analysis of the governing equations in the limit of very soft substrates predicts $\langle\hat{l}_c\rangle = \langle l_c/h_0\rangle \sim \mathscr{R}^{1/3}Ca^{-1/3}$ and $\langle\hat{V}\rangle \sim \epsilon\mathscr{R}n^{-1}Ca^{-1}$ (*SI Appendix, section 7*). In other words, while the gliding speed is independent of the bacterial length in an elasticity-dominated regime, the gliding speed $\langle\hat{V}\rangle$ scales with the bacterial length as $1/n$ when capillary effects dominate. This scaling law is obtained by balancing the localized capillary force at the slime–air interface and the viscous friction over the entire bacteria. Although the thrust results from the capillary-induced pressure at the leading edge and is thus essentially independent of bacterial length, the friction coefficient, given by $I_3/\hat{V}$, depends on the cell geometry and increases with n. Hence, the resulting velocity decreases with n. The scaling laws given above are confirmed by computations of the full elasto-capillary–hydrodynamic equations, as shown in Figs. 6 and 7. As expected, we find $\langle\hat{l}_c\rangle \sim Ca^{-1/3}$ and $\langle\hat{V}\rangle \sim Ca^{-1}$ when the softness number is very large. The contrast between the elasticity-dominated and the capillarity-dominated regimes is emphasized in Fig. 7, which shows that $\langle\hat{V}\rangle$ is independent on the wavenumber for very stiff (small η) substrates, while $\langle\hat{V}\rangle \sim 1/n$ for very soft (large η) substrates.

The Elasto-Capillary–Hydrodynamic Model Predicts the Experimental Gliding Speeds of *M. xanthus* Cells on Agar Substrates of Varying Stiffness

To test the validity of our theory, we cultured *M. xanthus* cells in a rich casitone yeast extract (CYE) medium, spotted cell suspensions on agar gel pads, and measured the average gliding speed of A-motile cells on gels of different concentrations of agar, corresponding to different stiffnesses (*Materials and Methods*). A good fit of collected data obtained by various authors (62–64) shows that the increase of the shear modulus (G) with agar concentration ($\mathcal{C}_{\text{agar}}$) can be approximated by the empirical law: $G \approx 20(\mathcal{C}_{\text{agar}} - 0.1)^2$ kPa. Such power laws are more rigorously derived in the percolation theory for gels (65). After recording and postprocessing the myxobacteria motion for a sample of $m = 40$ cells, we obtained the mean and SE of the
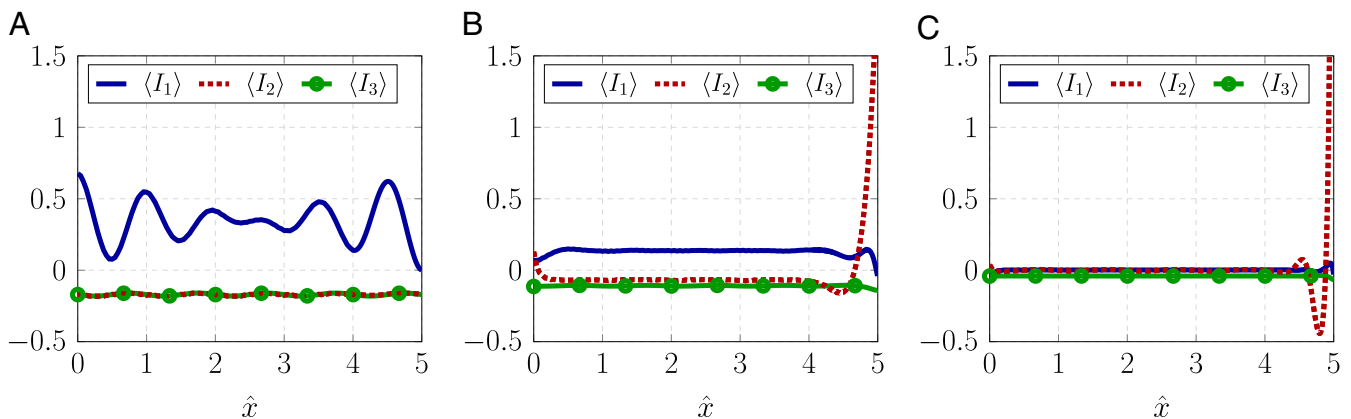

Fig. 5. Time-averaged distribution of the contributions I_1, I_2, and I_3 to the horizontal force balance for different values of η. The softness parameters are $\eta = 0.001$ (very stiff substrate) (*A*), $\eta = 5$ (mildly soft substrate) (*B*), and $\eta = 1000$ (very soft substrate) (*C*). Here, the input parameters are $\hat{A} = 0.25$, $n = 5$, $\hat{a} \approx 3.14 \times 10^{-3}$, and $Ca \approx 1.67 \times 10^{-3}$.
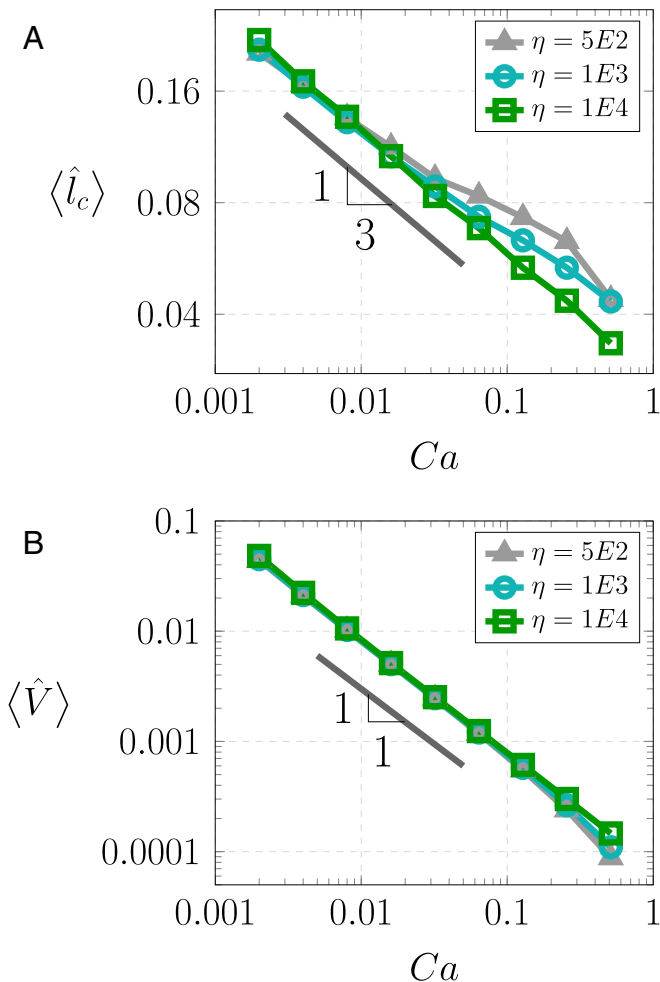
Fig. 6. Scaling with the capillary number of the horizontal length scale of the ridge (*A*) and the gliding speed (*B*), for different values of the softness parameter. Here, l_c is arbitrarily defined as the distance from the leading edge where the slope of the substrate first vanishes, i.e., $\frac{d\langle\hat{\delta}\rangle}{d\hat{x}}\left(\hat{x}=\frac{n}{2}-\hat{l}_c\right)=0$. Here, the input parameters are $\epsilon=0.008$, $\hat{A}=0.25$, $\hat{a}\approx3.14\times10^{-3}$, and $\mathscr{R}\simeq0.1$.

this mechanosensitive feature, we show in Movie S7 (also see *SI Appendix*, section 8.7), an animation showing a race between 2 cells gliding on substrates of softness number $\eta_1=7.9$ and $\eta_2=463$, corresponding to agar concentrations $\mathcal{C}_{\mathrm{agar}_1}\approx7\%$ and $\mathcal{C}_{\mathrm{agar}_2}\approx1\%$, respectively.

Table 1 shows that most of the parameter values (ℓ, L, A, C, h_0) used in comparison to our experimental data are in good agreement with the range of reported values concerning *M. xanthus* cells. However, there is lack of available data for slime properties measured directly underneath myxobacteria. To begin with, the slime thickness (5 nm) reported for *M. xanthus* cells is found in the wake of motile cells and not underneath (11). Therefore, it is very likely an underestimation of h_0, which is the actual mean slime thickness beneath the bacteria. Furthermore, our choice of $h_0=10$ nm is consistent with values used for *Flexibacter*, another bacteria with gliding motility, whose slime thickness ranges between 10 and 25 nm (25, 26). Regarding the material parameters specific to the slime, such as viscosity (μ) and surface tensions (γ_s, γ), the sources listed in Table 1 refer to experiments conducted on generic types of polysaccharide fluids, rather than myxobacterial slime. Nevertheless, one can argue that these slime characteristics listed in Table 1 also apply to myxobacteria cells, as it is believed that their slime is rich in polysaccharides (11). Our estimate of viscosity in Table 1 suggests that myxobacterial slime is a very viscous fluid, similar to other EPS concentrated fluids. Indeed, depending on the concentration of polysaccharides, viscosities have been reported as high as 5 to 20 Pa.s (36, 37). Concerning the slime–substrate surface tension γ_s, our estimate in Table 1 is found to be about half that of the interface between air and an agar substrate ($\sim$50 to 60 mN/m) (60, 66). However, experiments show that bacterial slime contains surfactants, indicating that the slime–substrate surface tension could be lower than that of the air–substrate tension. Indeed, it has been observed previously that polysaccharide–substrate tensions could be as low as $\sim$35 mN/m (67), which is in good agreement with our estimated value: $\gamma_s=30$ mN/m. A similar argument can be made for our estimate of γ, the slime–air interfacial tension, which is much lower than that of the air–water interface ($\sim$70 mN/m; ref. 67). Here as well, there is experimental evidence that lipopolysaccharides can reduce the surface tension down to values as low as 10 mN/m (69, 70), in reasonable agreement with the value used in our model.

gliding speed as shown in Fig. 8. The experimental data show a good agreement with the prediction of our model when we use the parameter values given in Table 1.

Experimental data in Fig. 8 confirm the existence of a 2-regime behavior of the average gliding speed as a function of agar concentration. At low agar concentrations, i.e., at low substrate stiffness, the gliding motion is due to capillary effects localized at the tip of the bacteria whose velocity follows the prediction of the asymptotic speed given by Eq. **13**. As the concentration increases, the substrate gets stiffer and capillary effects at its surface decrease in favor of elastic ones in the bulk. The substrate being stiffer, it becomes harder to deform and causes the oscillations of the bacterial shape to be rather converted into variations of the slime pressure along the bacteria. Thus, there is a gradual switch in the nature of the gliding thrust, from a localized pressure gradient toward the slime–air interface to a distributed slime pressure over the bacteria. As the substrate becomes stiffer with the concentration, the slime pressure based thrust increases, leading to higher gliding speeds. Fig. 8 shows that beyond a critical agar concentration of $\sim$5%, myxobacterial gliding speed increases considerably. In order to illustrate
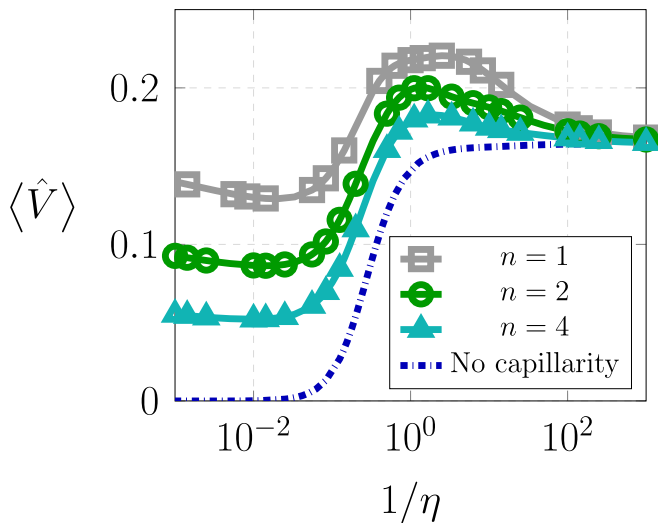

Fig. 7. Time-averaged gliding speed as a function of the softness parameter for different dimensionless bacterial lengths. Here, the input parameters are $\epsilon=0.008$, $\hat{A}=0.25$, $\mathscr{R}\approx0.1$, and $Ca\approx1.67\times10^{-3}$.
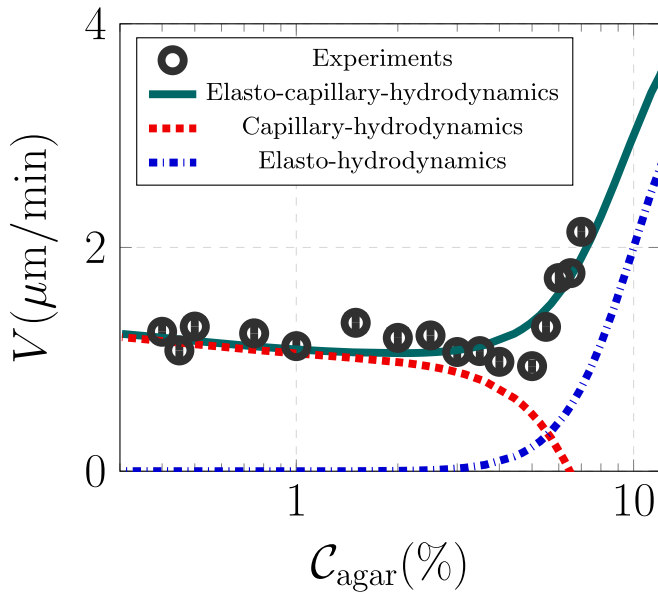
Fig. 8. Mean velocity of A-motile *M. xanthus* cells as a function of the concentration of agar in the substrate. The experimental data (symbols) are reported in terms of the mean values with an error bar corresponding to the SE, i.e., the uncertainty on the estimate of the mean. The dark green line corresponds to our simulations (see text for parameters) of the elasto-capillary–hydrodynamic problem. The blue dash-dot line corresponds to the case of a pure elastic substrate, while the red dash line is the asymptotic solution given by Eq. **13** for a very soft substrate.

To assess the robustness of our model to the parameter values listed in Table 1, we investigated how 20% modifications of these numbers influence our predicted speed–stiffness curve (*SI Appendix*, section 9). Our sensitivity analysis shows that these variations of the parameter values not only result in minor quantitative changes of the $V = f(\mathcal{C}_{\mathrm{agar}})$ curve, but they do not alter the (experimentally observed) existence of 2 regimes for gliding cells of soft substrates. Therefore, the emergence of gliding motility mechanisms from the interplay between elastic, capillary, and viscous forces is a rather robust theory, independent of the values of the model parameters.

Discussion

We have presented a model for the gliding of single myxobacteria cells and their underlying substrate. It appears that the dynamics of motor complexes can be modeled as a traveling wave, while the secreted slime serves as a lubricating film mediating the cell-substrate coupling. Our analysis shows that the mechanosensitivity of myxobacteria to their substrate results from their need to glide under drag-free and lift-free constraints.

We find that satisfying these constraints can lead to different balances between the viscous, capillary and elastic forces depending on the substrate stiffness. This leads to a 2-regime behavior of the gliding velocity. On very soft substrates, the motility thrust is due to the existence of a localized capillary-induced pressure gradient toward the slime–air interface. However, for much stiffer substrates, it originates from oscillations of the slime pressure in phase with the shape deformations over the bacteria length.

As a final calculation, we can estimate the thrust $\mathcal{T}$ required for the propulsion of a single myxobacteria cell. On substrates with $\mathcal{C}_{\mathrm{agar}} \leq 3\%$, the motility thrust is balanced by the friction I_3 exerted by the slime on the cell, and consequently, it was calculated as (in dimensional form) $\mathcal{T} \approx 2R\mu \int_0^\ell \frac{V}{h-\delta} \, dx \sim 2R\ell \frac{\mu V}{h_0}$, where $R \simeq 250$ nm is the radius of the rod-shaped bacteria. Using the parameters given above, along with $V \approx 1\,\mu m/min$, we obtain $\mathcal{T} \approx 196$ pN. This value is in good agreement with other experimental and computational estimates (~ 50 to 150 pN) of the propulsive force of single A-motile cells (30, 72) and S-motile cells (73, 74) (which move at approximately the same speed).

In conclusion, the speed–stiffness relationship investigated in this work improves our understanding of friction and substrate-mediated interaction between bacteria in a swarm of cells proliferating in soft media (75). A crucial next step would be to consider the actual shape of the cell and its modification under the torque exerted both by the outside slime pressure and by the inner aggregation of motor complexes at the so-called focal-adhesion sites (15, 23). It is possible that binding and unbinding of focal-adhesion complexes to the substrate may produce a traveling wave disturbance on the outer membrane of the cell. These membrane deformations may be due to the differences in the distance between the cell and the substrate in the bound and unbound states (76). Tackling such problems will require determining stable 3-dimensional deformations of the bacterial curved surface using membrane mechanics (77) and could give insight in the shape–motility coupling of other rod-shaped cells. This will also enable direct connections with physical aspects of force transduction from the bacterial motors.

Materials and Methods

Governing Equations. We model the bacterial slime as a newtonian viscous fluid and the substrate as a linear elastic solid (see *SI Appendix*, sections 1 and 2 for details). The slime being confined to a thin layer between the bacterial membrane and the substrate, its governing equations are obtained within the lubrication approximation. In the reference frame of the bacteria, the slime velocity component in the (horizontal) gliding direction reads (see *SI Appendix*, section 1.2 for derivation)

$$u_x(x,z,t) = \frac{1}{2\mu} \frac{\partial p}{\partial x}(z-h)(z-\delta) + V\frac{z-h}{h-\delta}, \qquad [14]$$

Table 1. List and values of the parameters used for comparing the elasto-capillary–hydrodynamic model to experiments

Parameters symbols	Definition	Model values	Experimentally reported values	Refs.
ℓ	Bacterial total length	5 μm	4 to 10 μm	24, 32, 71
L	Wavelength of membrane deformation	1 μm	0.7 to 1.5 μm	17, 24
A	Amplitude of membrane deformation	3 nm	3 to 5 nm	32
C	Speed of traveling motors	320 nm/s	100 to 1,000 nm/s	17
h_0	thickness of slime film	10 nm	5 to 25 nm	11, 26
μ	viscosity of slime film	47 Pa.s	5 to 20 Pa.s	36, 37
a	thickness of slime–air interface	1 nm	O (nm)	56, 57
γ_s	slime–substrate surface tension	30 mN/m	35 to 60 mN/m	60, 66, 67
γ	slime–air surface tension	4.8 mN/m	~ 10 mN/m	69, 70

where p is the slime pressure, δ the substrate deformation, and V the bacterial gliding speed. Moreover, the slime is treated as an incompressible fluid, where its velocity components are such that

$$\frac{\partial u_x}{\partial x} + \frac{\partial u_z}{\partial z} = 0, \qquad [15]$$

with $u_z(x, z, t)$ the vertical component of the slime velocity. By substituting Eq. **14** into Eq. **15** and integrating the resulting equation from the substrate surface ($z = \delta$) to the bacterial membrane ($z = h$), we obtain the following modified Reynolds equation (see *SI Appendix*, section 1.2 for derivation) (41):

$$-\frac{\partial}{\partial t}(h - \delta) + \frac{\partial}{\partial x}\left[\frac{1}{12\mu}\frac{\partial p}{\partial x}(h - \delta)^3 + \frac{1}{2}V(h - \delta)\right] = 0. \qquad [16]$$

In addition to Eq. **16**, the elasto-capillary–hydrodynamic problem of myxobacterial gliding on soft substrates is also governed by 1) an equation for the substrate deformation, 2) the lift-free and drag-free conditions, and 3) a force balance at the leading edge of the bacteria. Written in dimensionless form, these equations read respectively (*SI Appendix*, sections 6.1–6.4):

$$\frac{\partial}{\partial \hat{x}}\left[\frac{\partial \hat{p}}{\partial \hat{x}}(\hat{h} - \eta\hat{\delta})^3 + 6(\hat{V} - 2)(\hat{h} - \eta\hat{\delta})\right] = 0, \qquad [17a]$$

$$\hat{\delta}(\hat{x}, \hat{t}) - \frac{1}{\pi}\int_{-n/2}^{n/2}\hat{p}(\hat{x}', \hat{t})\ln\left(|\hat{x} - \hat{x}'| + \xi/\pi\right)d\hat{x}' = 0, \qquad [17b]$$

$$\int_{-n/2}^{n/2}\hat{p}(\hat{x}, \hat{t})d\hat{x} = 0, \qquad [17c]$$

$$-\int_{-n/2}^{n/2}\left(\hat{p}\frac{\partial \hat{b}}{\partial \hat{x}} + \frac{1}{2}\frac{\partial \hat{p}}{\partial \hat{x}}\left(\hat{h} - \eta\hat{\delta}\right) + \frac{\hat{V}}{\hat{h} - \eta\hat{\delta}}\right)d\hat{x} = 0, \qquad [17d]$$

$$\hat{p}(n/2, \hat{t}) = -\frac{\epsilon/Ca}{\hat{h}(n/2) - \eta\hat{\delta}(n/2)} \times$$
$$\left(2\sqrt{1 + \left[\mathscr{R}\frac{\xi}{2\hat{a}}\ln\left(1 + \frac{2\hat{a}}{\xi}\right)\right]^2} - 2\right)^{1/2}. \qquad [17e]$$

Note that we use the traveling wave ansatz in dimensionless form, i.e., $\frac{\partial \hat{h}}{\partial \hat{t}} = \frac{\partial \hat{h}}{\partial \hat{x}}$, to rewrite Eq. **16** as Eq. **17a**. In the absence of capillarity effects, the governing equations for the elasto-hydrodynamic problem are obtained by taking the limit $\xi \to 0$ of Eq. **17** above (*SI Appendix*, section 6.5).

Numerical Treatment. The Reynolds equation governing the viscous slime beneath the bacteria is a nonlinear equation as readily seen by the cubic power in Eq. **17a**. Therefore, we use an iterative Newton method to obtain the slime pressure field, the substrate deformation, the bacterial gliding speed, and the leading-edge pressure (*SI Appendix*, sections 5.1 and 8.1). This algorithm consists in starting with a guess solution $\mathbf{q}_0$ and then linearizing the governing equations around $\mathbf{q}_0$ and inverting the resulting linear system to find an increment $\delta\mathbf{q}$ with which $\mathbf{q}_0$ is updated into $\mathbf{q}_1 = \mathbf{q}_0 + \delta\mathbf{q}$, the subscripts referring to the Newton iteration step. Now, assigning to $\mathbf{q}_1$

the role of $\mathbf{q}_0$, the process of linearizing, inverting and updating the solution is repeated until the norm of the increment is smaller than a tolerance that we set to $\sim 10^{-10}$ (*SI Appendix*, sections 5.1 and 8.1).

The linearized equations obtained at each Newton iteration are solved using the finite element method (78). We implemented this numerical method via FreeFem++ (79), a finite element solver that requires rewriting the governing equations in a weak form, discretizing the computational domain, expanding the unknown of the problem in a basis of shape functions, and inverting the resulting discrete linear system. All of the details regarding the weak form, the choice of shape functions, and the convergence verification of the discrete problem are given in *SI Appendix*, sections 5.1–5.3 and 8.1–8.3. Using the aforementioned method, we solve numerically, for given values of the set of parameters (η, Ca, $\mathscr{R}$, n, $\hat{A}$, ϵ, $\hat{a}$), the elasto-capillary–hydrodynamic problem at different time instants $\hat{t}$ and obtain instantaneous and time-averaged values of the slime pressure, the substrate deformation, and the bacterial gliding speed.

In order to illustrate the importance of the forces at play (Fig. 5) and the velocity as a function of the softness parameter (Fig. 7) in the presence of capillary effects, we chose the capillary number $Ca \approx 1.67 \times 10^{-3}$. Although somewhat arbitrary, this value of Ca is convenient for 2 reasons. On the one hand, as shown in *SI Appendix*, Fig. S16, smaller values of Ca lead to smaller capillary effects at the leading edge and do not serve well in our aim of emphasizing the importance of capillarity. On the other hand, higher values of Ca would lead to a more confined elasto-capillary ridge whose width scales as $\sim Ca^{-1/3}$, as shown by Fig. 6B. Such highly confined ridges are challenging to accurately resolve numerically, as discussed in *SI Appendix*, section 8.3 on mesh convergence. Therefore, the value of Ca we chose to illustrate the effects of capillarity on gliding motility is a good compromise. Nevertheless, this value is also relevant for experiments on myxobacteria. Indeed, by using our best estimates of *M. xanthus* parameters, listed in Table 1, we find a rather close value: $Ca \approx 3.13 \times 10^{-3}$.

The codes used for our simulations have been deposited in the GitHub repository, https://github.com/mandadapu-group/myxoglide.

Experimental Method. TIRF microscopy images were captured using a Hamamatsu ImageEM X2 EM-CCD camera C9100-23B (pixel size, 160 nm) on an inverted Nikon Eclipse-Ti microscope with a 100×1.49 numerical aperture TIRF objective. Gliding velocities of *M. xanthus* cells were measured on CYE agar pads containing small to moderate concentrations of agar. For agar concentrations higher than 7%, it becomes very difficult to synthesize homogeneous substrates. To avoid potential interference of twitching motility, we used a *pilA⁻* strain that was unable to move by twitching due to the absence of pili. Moreover, to avoid potential interference of cell collisions, cell culture was diluted to the point where cells did not interact with one another. For each agar concentration, 20-min time-lapse videos were recorded with a ZEISS AXIO microscope and a ZEISS AxioCam MRm camera at 20-s intervals, and, for a given agar concentration, the velocities of 40 cells were calculated using ImageJ.

1. M. C. Van Loosdrecht, J. Lyklema, W. Norde, A. J. Zehnder, Influence of interfaces on microbial activity. *Microbiol. Rev.* **54**, 75–87 (1990).
2. M. Fletcher, Bacterial biofilms and biofouling. *Curr. Opin. Biotechnol.* **5**, 302–306 (1994).
3. J. W. Costerton, Z. Lewandowski, D. E. Caldwell, D. R. Korber, H. M. Lappin-Scott, Microbial biofilms. *Annu. Rev. Microbiol.* **49**, 711–745 (1995).
4. A. Persat *et al.*, The mechanical world of bacteria. *Cell* **161**, 988–997 (2015).
5. D. B. Kearns, A field guide to bacterial swarming motility. *Nat. Rev. Microbiol.* **8**, 634–644 (2010).
6. J. Munoz-Dorado, F. J. Marcos-Torres, E. Garcia-Bravo, A. Moraleda-Munoz, J. Pérez, Myxobacteria: Moving, killing, feeding, and surviving together. *Front. Microbiol.* **7**, 781 (2016).
7. B. Nan, D. R. Zusman, Uncovering the mystery of gliding motility in the myxobacteria. *Annu. Rev. Genet.* **45**, 21–39 (2011).
8. W. Shi, D. R. Zusman, The two motility systems of *Myxococcus xanthus* show different selective advantages on various surfaces. *Proc. Natl. Acad. Sci. U.S.A.* **90**, 3378–3382 (1993).
9. M. Fontes, D. Kaiser, Myxococcus cells respond to elastic forces in their substrate. *Proc. Natl. Acad. Sci. U.S.A.* **96**, 8052–8057 (1999).
10. B. Ladoux, A. Nicolas, Physically based principles of cell adhesion mechanosensitivity in tissues. *Rep. Prog. Phys.* **75**, 116601 (2012).
11. A. Ducret, M.-P. Valignat, F. Mouhamar, T. Mignot, O. Theodoly, Wet-surface-enhanced ellipsometric contrast microscopy identifies slime as a major adhesion factor during bacterial surface motility. *Proc. Natl. Acad. Sci. U.S.A.* **109**, 10036–10041 (2012).
12. C. Wolgemuth, E. Hoiczyk, D. Kaiser, G. Oster, How myxobacteria glide. *Curr. Biol.* **12**, 369–377 (2002).
13. J. Hodgkin, D. Kaiser, Genetics of gliding motility in *Myxococcus xanthus* (myxobacterales): Two gene systems control movement. *Mol. Gen. Genet.* **171**, 177–191 (1979).
14. M. J. McBride, Bacterial gliding motility: Multiple mechanisms for cell movement over surfaces. *Annu. Rev. Microbiol.* **55**, 49–75 (2001).
15. L. M. Faure, *et al.*, The mechanism of force transmission at bacterial focal adhesion complexes. *Nature* **539**, 530–535 (2016).
16. J. Xing, F. Bai, R. Berry, G. Oster, Torque–speed relationship of the bacterial flagellar motor. *Proc. Natl. Acad. Sci. U.S.A.* **103**, 1260–1265 (2006).
17. B. Nan *et al.*, Flagella stator homologs function as motors for myxobacterial gliding motility by moving in helical trajectories. *Proc. Natl. Acad. Sci. U.S.A.* **110**, E1508–E1513 (2013).

18. K. K. Mandadapu, J. A. Nirody, R. Berry, G. Oster, Mechanics of torque generation in the bacterial flagellar motor. *Proc. Natl. Acad. Sci. U.S.A.* **112**, 4381–4389 (2015).
19. G. Fu et al., MotAB-like machinery drives the movement of MreB filaments during bacterial gliding motility. *Proc. Natl. Acad. Sci. U.S.A.* **115**, 2484–2489 (2018).
20. R. N. Doetsch, G. J. Hageage, Motility in procaryotic organisms: Problems, points of view, and perspectives. *Biol. Rev.* **43**, 317–362 (1968).
21. R. P. Burchard, Gliding motility of prokaryotes: Ultrastructure, physiology, and genetics. *Annu. Rev. Microbiol.* **35**, 497–529 (1981).
22. S. E. Spagnolie, E. Lauga, Jet propulsion without inertia. *Phys. Fluids* **22**, 081902 (2010).
23. T. Mignot, J. W. Shaevitz, P. L. Hartzell, D. R. Zusman, Evidence that focal adhesion complexes power bacterial gliding motility. *Science* **315**, 853–856 (2007).
24. B. Nan et al., Myxobacteria gliding motility requires cytoskeleton rotation powered by proton motive force. *Proc. Natl. Acad. Sci. U.S.A.* **108**, 2498–2503 (2011).
25. R. W. O'Brien, The gliding motion of a bacterium: Flexibacter strain BH3. *J. Aust. Math. Soc.* **23**, 2–16 (1981).
26. A. M. Siddiqui, R. P. Burchard, W. H. Schwarz, An undulating surface model for the motility of bacteria gliding on a layer of non-Newtonian slime. *Int. J. Non Linear Mech.* **36**, 743–761 (2001).
27. Y. Wang, T. Hayat, A. M. Siddiqui, Gliding motion of bacteria on a power-law slime. *Math. Methods Appl. Sci.* **28**, 329–347 (2005).
28. N. Ali, Z. Asghar, O. Anwar Bég, M. Sajid, Bacterial gliding fluid dynamics on a layer of non-Newtonian slime: Perturbation and numerical study. *J. Theor. Biol.* **397**, 22–32 (2016).
29. D. J. Lemon, X. Yand, P. Srivastava, Y. Y. Luk, A. G. Garza, Polymertropism of rod-shaped bacteria: Movement along aligned polysaccharide fibers. *Sci. Rep.* **7**, 7643 (2017).
30. R. Balagam et al., *Myxococcus xanthus* gliding motors are elastically coupled to the substrate as predicted by the focal adhesion model of gliding motility. *PLoS Comput. Biol.* **10**, e1003619 (2014).
31. E. M. F. Mauriello et al., Bacterial motility complexes require the actin-like protein, MreB and the Ras homologue, MglA. *EMBO J.* **29**, 315–326 (2010).
32. A. E. Pelling, Y. Li, W. Shi, J. K. Gimzewski, Nanoscale visualization and characterization of *Myxococcus xanthus* cells with atomic force microscopy. *Proc. Natl. Acad. Sci. U.S.A.* **102**, 6484–6489 (2005).
33. B. Nan, D. R. Zusman, Novel mechanisms power bacterial gliding motility. *Mol. Microbiol.* **101**, 186–193 (2016).
34. R. Yu, D. Kaiser, Gliding motility and polarized slime secretion. *Mol. Microbiol.* **63**, 454–467 (2007).
35. M. L. Gibiansky, W. Hu, K. A. Dahmen, W. Shi, G. C. L. Wong, Earthquake-like dynamics in *Myxococcus xanthus* social motility. *Proc. Natl. Acad. Sci. U.S.A.* **110**, 2330–2335 (2013).
36. J. H. Choi, D. K. Oh, J. H. Kim, J. M. Lebeault, Characteristics of a novel high viscosity polysaccharide, methylan, produced by methylobacterium organophilum. *Biotechnol. Lett.* **13**, 417–420 (1991).
37. Y. Isobe, K. Endo, H. Kawai, Properties of a highly viscous polysaccharide produced by a bacillus strain isolated from soil. *Biosci. Biotechnol. Biochem.* **56**, 636–639 (1992).
38. E. M. Purcell, Life at low Reynolds number. *Am. J. Phys.* **45**, 3 (1977).
39. J. Happel, H. Brenner, *Low Reynolds Number Hydrodynamics* (Martinus Nijhoff Publishers, 1983).
40. O. Reynolds, On the theory of lubrication and its application to Mr Beauchamp tower's experiments, including an experimental determination of the viscosity of olive oil. *Phil. Trans. R. Soc. Lond.* **177**, 157–234 (1886).
41. L. G. Leal, *Advanced Transport Phenomena: Fluid Mechanics and Convective Transport Processes* (Cambridge University Press, 2007), pp. 306–315.
42. M. Sun, M. Wartel, E. Cascales, J. W. Shaevitz, T. Mignot, Motor-driven intracellular transport powers bacterial gliding motility. *Proc. Natl. Acad. Sci. U.S.A.* **108**, 7559–7564 (2011).
43. O. A. Croze, G. P. Ferguson, M. E. Cates, W. C. K. Poon, Migration of chemotactic bacteria in soft agar: Role of gel concentration. *Biophys. J.* **101**, 525–534 (2011).
44. V. T. Nayar, J. D. Weiland, C. S. Nelson, A. M. Hodge, Elastic and viscoelastic characterization of agar. *J. Mech. Behav. Biomed. Mater.* **7**, 60–68 (2012).
45. K. L. Johnson, *Contact Mechanics* (Cambridge University Press, 1985), pp. 1–20.
46. J. M. Skotheim, L. Mahadevan, Soft lubrication. *Phys. Rev. Lett.* **92**, 245509 (2004).
47. J. M. Skotheim, L. Mahadevan, Soft lubrication: The elastohydrodynamics of nonconforming and conforming contacts. *Phys. Fluids* **17**, 092101 (2005).
48. G. I. Taylor, Analysis of the swimming of microscopic organisms. *Proc. R. Soc. Lond. A* **209**, 447–461 (1951).
49. E. Lauga, W. R. DiLuzio, G. M. Whitesides, H. A. Stone, Swimming in circles: Motion of bacteria near solid boundaries. *Biophys. J.* **90**, 400–412 (2006).
50. O. S. Pak, E. Lauga, "Theoretical models of low-Reynolds-number locomotion" in *Fluid-Structure Interactions in Low-Reynolds-Number Flows*, C. Duprat, H. A. Stone, Eds. (The Royal Society of Chemistry, 2016), pp. 100–135.
51. M. Argentina, J. M. Skotheim, L. Mahadevan, Settling and swimming of flexible fluid-lubricated foils. *Phys. Rev. Lett.* **99**, 224503 (2007).
52. D. F. Katz, On the propulsion of micro-organisms near solid boundaries. *J. Fluid Mech.* **64**, 33–49 (1974).
53. M. E. R. Shanahan, P. G. de Gennes, L'arête produite par un coin liquide près de la ligne triple de contact solide/liquide/fluide [in French]. *C. R. Acad. Sci. Paris* **302**, 517–521 (1986).
54. M. E. R. Shanahan, The spreading dynamics of a liquid drop on viscoelastic solid. *J. Phys. D Appl. Phys.* **21**, 981–985 (1988).
55. A. Marchand, S. Das, J. H. Snoeijer, B. Andreotti, Contact angles on a soft solid: From young's law to Neumann's law. *Phys. Rev. Lett.* **109**, 236101 (2012).
56. L. A. Lubbers et al., Drops on soft solids: Free energy and double transition of contact angles. *J. Fluid Mech.* **747**, 1 (2014).
57. R. W. Style, A. Jagota, C. Y. Hui, E. R. Dufresne, Elastocapillarity: Surface tension and the mechanics of soft solids. *Annu. Rev. Cond. Mat. Phys.* **8**, 99–118 (2017).
58. L. Limat, Straight contact lines on a soft incompressible solid. *Eur. Phys. J. E.* **35**, 134 (2012).
59. J. Dervaux, L. Limat, Contact lines on soft solids with uniform surface tension: Analytical solutions and double transition for increasing deformability. *Proc. R. Soc. Lond.* **471**, 20140813 (2015).
60. Y. Yoshitake, S. Mitani, K. Sakai, K. Takagi, Surface tension and elasticity of gel studied with laser-induced surface-deformation spectroscopy. *Phys. Rev. E* **78**, 041405 (2008).
61. P. G. de Gennes, Wetting: Statics and dynamics. *Rev. Mod. Phys.* **57**, 827–863 (1985).
62. D. G. T. Strange, M. L. Oyen, Composite hydrogels for nucleus pulposus tissue engineering. *J. Mech. Behav. Biomed. Mater.* **11**, 16–26 (2012).
63. M. L. Oyen, Mechanical characterization of hydrogel materials. *Int. Mater. Rev.* **59**, 44–59 (2014).
64. B. Mao, "Dynamis of agar-based gels in contact with solid surfaces: Gelation, adhesion, drying and formulation," PhD thesis, Université de Bordeaux, Bordeaux, France (2017).
65. P. G. de Gennes, *Scaling Concepts in Polymer Physics* (Cornell University Press, New York, NY, 1979), pp. 137–142.
66. X. Shao, J. R. Saylor, J. B. Bostwick, Extracting the surface tension of soft gels from elastocapillary wave behavior. *Soft Matter* **14**, 7347–7353 (2018).
67. K. Prasad, K. P. Trivedi, A. K. Siddhanta, A. Bhattacharya, Surface tension and fluorescence studies of polysaccharide-surfactant solutions: Agar-CTAB. *Ind. J. Chem* **44**, 2445–2449 (2005).
68. M. Dworkin, K. H. Keller, D. Weisberg, Experimental observations consistent with a surface tension model of gliding motility of *Myxococcus xanthus. J. Bacteriol.* **155**, 1367–1371 (1983).
69. B. Kronberg, H. Holmberg, B. Lindman, "Surface active polymers," in *Surface Chemistry of Surfactants and Polymers* (Wiley-Blackwell, 2014), pp. 197–209.
70. T. Zhang, "Studies of DPPA & LPS monolayers on aqueous solutions by surface tensiometry and Brewster angle microscopy," MSc thesis, Ohio State University, Columbus, OH (2014).
71. F. Peruani et al., Collective motion and nonequilibrium cluster formation in colonies of gliding bacteria. *Phys. Rev. Lett.* **108**, 098102 (2012).
72. C. W. Wolgemuth, Force and flexibility of flailing myxobacteria. *Biophys. J.* **89**, 945–950 (2005).
73. M. Clausen, V. Jakovljevic, L. Sogaard-Andersen, B. Maier, High-force generation is a conserved property of type iv pilus system. *J. Bacteriol.* **191**, 4633–4638 (2009).
74. B. Sabass, M. Koch, G. Liu, H. A. Stone, J. Shaevitz, Force generation by groups of migrating bacteria. *Proc. Natl. Acad. Sci. U.S.A.* **114**, 7266–7271 (2017).
75. A. Gallegos, B. Mazzag, A. Mogilner, Two continuum models for the spreading of myxobacteria swarms. *Bull. Math. Biol.* **68**, 837–861 (2006).
76. A. Carlson, L. Mahadevan, Elastohydrodynamics and kinetics of protein patterning in the immunological synapse. *PLoS Comput. Biol.* **11**, e1004481 (2015).
77. A. Sahu, R. A. Sauer, K. K. Mandadapu, Irreversible thermodynamics of curved lipid membranes. *Phys. Rev. E* **96**, 042409 (2017).
78. O. C. Zienkiewicz, R. L. Taylor, *The Finite Element Method* (McGraw-Hill, 1991).
79. F. Hecht, New development in FreeFem++. *J. Num. Math.* **20**, 251–265 (2012).